Available online at www.sciencedirect.com
ScienceDirect
Polymer 49 (2008) 534–545
polymer
www.elsevier.com/locate/polymer

Kinetics of photopolymerization-induced phase separation and morphology development in mixtures of a nematic liquid crystal and multifunctional acrylate

Hatice Duran [a,1], Scott Meng [a,2], Namil Kim [a], Jun Hu [b], Thein Kyu [a,*], Lalgudi V. Natarajan [c], Vincent P. Tondiglia [c], Timothy J. Bunning [d]

[a] *Department of Polymer Engineering, University of Akron, Akron, OH 44325-0301, United States*
[b] *Department of Chemistry, University of Akron, Akron, OH 44325-3601, United States*
[c] *Science Applications International Corporation, Dayton, OH 45431, United States*
[d] *Air Force Research Laboratory, Materials and Manufacturing Directorate, Wright–Patterson Air Force Base, OH 45433, United States*

Received 10 August 2007; received in revised form 15 November 2007; accepted 18 November 2007
Available online 22 November 2007

Abstract

Photopolymerization behavior and reaction kinetics for a series of multifunctional acrylate monomer(s) and eutectic liquid crystal blends were investigated with particular emphasis on determination of the reaction rate coefficients for propagation and termination steps of photopolymerization. Reaction rate coefficients were determined via real-time infrared spectroscopy and compared with those obtained by photo-differential scanning calorimetry. Effects of various parameters such as LC concentration, light intensity, and monomer functionality on the kinetics were investigated. Phase transition temperature versus composition phase diagrams were established by means of optical microscopy and differential scanning calorimetry for mixtures of triacrylate/liquid crystal (LC) before photopolymerization and after exposing to ultra violet (UV) irradiation under various reaction times. The snapshot phase diagram of the reacting mixtures exhibited isotropic gel, isotropic liquid + nematic, and narrow pure nematic coexistence regions. These coexistence regions were further confirmed by morphological changes of the polymer dispersed liquid crystal films as functions of temperature and concentration using polarized optical microscopy.

Keywords: Photopolymerization-induced phase separation; Photoreaction kinetics; Real-time morphology development

1. Introduction

Polymer dispersed liquid crystals (PDLCs) are composite materials consisting of randomly distributed micron-sized liquid crystal droplets in a polymer matrix, formed by phase separation of the initially homogeneous liquid crystal–polymer mixture. A typical photocurable PDLC formulation contains at least a multifunctional monomer (e.g., acrylate or methacrylate), liquid crystal molecules and a photoinitiator mixture [1]. In acrylate based PDLC, LC phase separation occurs via polymerization-induced phase separation (PIPS) which is strongly dependent on gelation, polymer vitrification, polymerization kinetics, and system variables such as monomer, initiator, and temperature.

In a previous paper [2], we examined phase equilibria of binary mixtures of liquid crystal (E7) and multi-arm star acrylate monomer derivatives as a function of the number of acrylate arms. In the present study, the morphological development and phase separation kinetics subjected to photopolymerization will be investigated. It is well documented that the morphology exerts profound effects on the electro-optical properties of PDLC films [3–7]. In general, the emerged morphology is controlled by the interplay between polymerization rate and

* Corresponding author. Tel.: +1 330 9726672; fax: +1 330 2582339.
E-mail address: tkyu@uakron.edu (T. Kyu).
[1] Present address: Max Planck Institute for Polymer Research, Mainz DE-55128, Germany.
[2] Present address: Technical Solution Center, Excel Polymers, Burton, OH 44021, United States.

0032-3861/$ - see front matter © 2007 Elsevier Ltd. All rights reserved.
doi:10.1016/j.polymer.2007.11.039

phase separation dynamics, which depends on a number of variables such as LC concentration, monomer functionality, irradiation intensity, exposure time, and reaction temperature [8]. In addition, the selection of initial conditions (e.g., composition and temperature relative to the initial phase diagram of the starting mixture) can affect the final morphology and also quality of the PDCL film [9]. Using the starting monomer/LC diagram as a guide for photopolymerization, the effects of LC concentration, light intensity, and monomer functionality on the emergence of the domain morphology of the composites have been examined. Unlike previously reported studies [6,10,11], we experimentally monitored the LC structure formation during the photopolymerization in reference to the starting phase diagrams. In this way, it gives a more comprehensive view on the development of complex morphology when subjected to photopolymerization conditions. Of particular interest is that the final morphology strongly depends on the interplay between the rate of polymerization and phase separation kinetics guided by the starting phase diagram. Real-time infrared (RT-IR) instrument was used to determine the reaction rate coefficients, which are compared with those obtained by photo-differential scanning calorimetry.

2. Experimental section

2.1. Materials and sample preparation procedures

The multifunctional acrylate monomers utilized were trimethylolpropane triacrylate (TMPTA), pentaerythritol tetra-acrylate (PETA), and pentaerythritol penta-hexa-acrylate (DPEPHA) from Aldrich. The photocurable formulations contained a reactive monomer, a chain extender (*N*-vinyl pyrrolidone (NVP)), a eutectic liquid crystal mixture (E7) (EM Industries), a visible photoinitiator Rose Bengal acetate ester RBAX (Spectra group), a surfactant octanoic acid (Sigma–Aldrich), and a co-initiator (*N*-phenyl glycine (NPG)). The multifunctional monomer and E7 blends were prepared by mixing the desired amount of E7 in the monomer matrix using ~17 wt% photoinitiator syrups. RBAX photoinitiator has two broad absorptions in the regions of 350–440 nm and 450–560 nm [12,13]. Its molar extinction coefficients at 365 and 532 nm are 1487 and 2441 $l\,mol^{-1}\,cm^{-1}$, respectively [14], which allow photopolymerization reactions at either or both wavelengths. Blends of E7/multifunctional acrylate(s)/photoinitiator were prepared by weighing and mixing without requiring any solvent, the appropriate amounts of multifunctional acrylates and E7 in small vials. The blends were then rigorously stirred with magnetic stirrers. Following mechanical stirring, all samples were further sonicated for approximately 1 h in a sonic bath (Branson 2200) to ensure thorough mixing.

2.2. Establishment of experimental phase diagrams

2.2.1. Phase diagram for uncured monomer/LC mixtures

In the optical microscopic experiment, a Nikon Optipot 2-POL microscope with a filtered Halogen light source (12 V, 100 W) was utilized with various lens magnifications ranging from 10× to 50×. A sample hot stage (Linkam Scientific Instruments, Model TS1500), connected to a programmable temperature controller (Linkam, Model TMS93) and a cooling system (Model LNP93/2) was used. Samples were sandwiched between cover glass slides yielding a thickness ranging between 10 and 15 μm. Samples covered with glass slides were heated until the materials became optically isotropic, and then cooled down slowly. Subsequently, the samples were reheated to their isotropic states and the experiment was repeated to check for reproducibility. The heating and cooling rates were 0.5 °C/min unless indicated otherwise. During cooling, the temperature at which birefringent droplets first appeared was recorded as T_{NI} for each mixture. The disappearance of all birefringent entities was regarded as the isotropic (I) temperature of each mixture during heating. Once the phase transition and/or phase separation temperature was observed approximately, then a temperature ramp experiment was carried out from slightly above the isotropic temperature of the mixture to two-phase regions and vice versa in order to find the phase transition temperature.

Regarding the differential scanning calorimetric (DSC) experiment, TA Instruments (Model Q1000) Thermal Analyzer equipped with a cooling chamber was used in conjunction with liquid nitrogen as a purging and cooling medium. The DSC peak was taken as the nematic–isotropic phase transition temperature (T_{NI}). Three different rates (2, 3, and 5 °C/min) were utilized and then the T_{NI} of each mixture was determined by extrapolating the T_{NI} values to the zero heating rate. This procedure may yield a closer value to that of the equilibrium, since both constituents are small molecule systems, but it is by no means in equilibrium. Samples in the recommended amount of 5–10 mg were sealed in hermetic pans. DSC experiments were performed in the temperature range of −30 to 70 °C to determine the nematic–isotropic transitions of the neat E7 and of its blends with multifunctional acrylate containing no curing agent.

2.2.2. Phase diagram for polymer/LC mixtures

In order to examine the shift of the coexistence line in the phase diagram driven by photopolymerization, monomer/LC/initiator mixture was first polymerized in hermetic aluminum pans via photo-differential calorimetry (P-DSC; see Section 2.3 for detailed explanation) and then subjected to UV illumination at an intensity of 50 mW/cm^2 for various exposure times (0, 6, 12, 30 and 60 s). Subsequently, the nematic–isotropic transition temperature, T_{NI}, in the cured films was measured by DSC similar to the uncured monomer/LC mixtures.

2.3. Photo-differential scanning calorimetry

Reaction rates were determined using a photo-differential scanning calorimeter (P-DSC Q1000, Thermal analysis) instrument equipped with a dual beam photo-calorimetric accessory and a lid specially designed for the photochemical reaction measurements. Each blend of monomer/E7 weighing 3–5 mg was placed in a hermetic aluminum DSC pan. An

empty DSC pan was used as reference. The sample weights and initiator concentrations were adjusted to form a thin film with a uniform thickness so that the sample can receive uniform light intensity and the Beer–Lambert law is obeyed. Prior to the UV irradiation, the P-DSC cell was flushed with nitrogen gas for about 5 min in order to prevent from moisture absorption and/or oxidation of the sample. The sample temperature was then adjusted to the required temperature for the UV exposure by a medium-pressure mercury lamp equipped with a 365 nm band-pass filter. Three different intensities (i.e., 44.5, 70, and 150 mW/cm^2) were employed for the investigation of the effect of the UV intensity on the photopolymerization kinetics. Similar experiments were carried out at three different temperatures (30, 40 and 50 °C) in order to determine the effect of curing temperature on the photopolymerization kinetics.

The real-time photo-induced polymerization rate was measured from the temporal change reaction heat flux as a function of time, since the rate of polymerization, R_p, is proportional to the number of monomer units reacted [15], the heat flow may be expressed as

$$R_p = \frac{dH}{dt}\frac{[M]}{\Delta H_0 n}\left(\mathrm{mol\,l^{-1}\,s^{-1}}\right) \quad (1)$$

where dH/dt is the heat flow in J mol^{-1} s^{-1}, [M] is the monomer concentration in mol l^{-1}, and n is the number of double bonds per monomer molecule. ΔH_0 is the standard heat of polymerization, which is ca. 80 kJ mol^{-1} [16]. The heat released under complete polymerization of 1 mol of a multifunctional acrylate, ΔH_{ideal}, was calculated in accordance with the following relation,

$$\Delta H_{ideal} = \frac{n\Delta H_0}{M_w}(\mathrm{kJ/g}) \quad (2)$$

where M_w is the molecular weight of monomer in g mol^{-1}. Once the value for the heat of polymerization was determined, then the percent conversion may be calculated from the ratio of the theoretical (ideal) heat generated to the measured heat of polymerization for full conversion of the monomer in what follows:

$$\alpha = \frac{\Delta H_p}{\Delta H_{ideal}} \quad (3)$$

2.4. Real-time infrared spectroscopy

The fast response of the IR detector facilitates the determination of the maximum photoreaction rate, which was reached within 30 ms of UV exposure as compared to 3 s for P-DSC analysis [17]. More importantly, this spectroscopic technique permits in situ monitoring of the chemical processes via mimicking the disappearance of the characteristic bands of the reactive monomer subjected to UV exposure [18–21]. A RT-IR spectrophotometer (Thermo Nicolet model Nexus 870) equipped with an IR detector (model DTGS-TEC) was used. Omnic series software was utilized for data acquisition, whereas Engauge Digitizer 2.3 software was used for data analysis. RT-IR instrument was modified to provide nitrogen environment in a sealed glass reactor cell equipped with quartz windows and to control the chamber temperature (Fig. 1). Samples were exposed to either UV or green laser light through the quartz windows with the aid of an optical fiber cable.

Two different light sources were utilized: an UV source (Linos Photonics, LQ UV1000) with 40 mW/cm^2 intensity at 365 nm and a green laser (19 mW/cm^2) for photopolymerization at 532 nm. Thin films of monomer were prepared by sandwiching a very small amount of monomer/LC/initiator mixture with a uniform thickness of 20 μm between two quartz plates. The reasons for the need of thin films are first to minimize the attenuation of light so that the Beer–Lambert law is obeyed and to receive a uniform light illumination. Second, the film thickness must be adjusted to be sufficiently thin so that the infrared absorbance of the double bonds is quantifiable in the initial stage. Finally, the polymerization reactions are highly exothermic, which can lead to a local temperature rise especially in thick films that further complicates the kinetic analysis.

The film sample was placed in the aforementioned IR spectrometer chamber, and subsequently exposed to the curing (UV or laser) beam in order to trigger the polymerization. Subsequently, the reduction in the IR absorbance of the acrylate double bonds at 804 cm^{-1} (C=C stretching) was monitored to determine the polymerization rate. The conversion of the acrylate functional group at a given time was calculated from the absorbance before $(A_{804})_0$ and after $(A_{804})_t$ the exposure to UV light according to the following equation,

$$\alpha(t) = \frac{(A_{804})_{t0} - (A_{804})_t}{(A_{804})_{t0}} \quad (4)$$

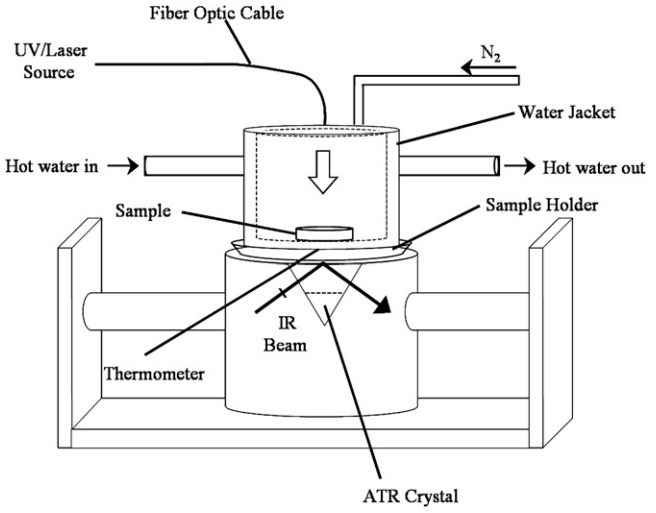

Fig. 1. Schematic representation of the modified set-up for real-time IR equipped with the UV/laser source.

The decline in the acrylate double-bond absorbance can be directly related to the rate of polymerization (R_p) in accordance with the following relation:

$$R_p = [M]_0 \frac{(A_{804})_{t0} - (A_{804})_t}{(A_{804})_{t0}(\Delta t)} \tag{5}$$

where $[M]_0$ is the initial monomer concentration and Δt is the time increment from the beginning of photopolymerization. The individual reaction rate coefficients (k_t and k_p) were measured as a function of conversion by irradiating for some times and subsequently stopping the UV irradiation for the dark reaction to proceed.

3. Calculation of theoretical phase diagram

The total free energy of liquid crystal/reactive monomer mixtures can be described in terms of a combined Flory–Huggins (g^{FH}) and Maier–Saupe (g^{MS}) theory, viz., $g = g^{FH} + g^{MS}$. The free energy density of Flory–Huggins for isotropic mixing with a reactive monomer is expressed as [22,23]

$$g^{FH} = \frac{G^{FH}}{nkT} = \frac{\phi_1}{r_1}\ln\phi_1 + \frac{\phi_m}{r_m}\ln\phi_m + \frac{\phi_p}{r_p}\ln\phi_p + \chi_{aa}\phi_1(1-\phi_1) \tag{6}$$

where subscripts 1, m, and p refer to liquid crystal, reactive acrylate monomer, and polymer formed after polymerization and kT represents thermal energy with k being the Boltzmann constant. The FH interaction parameter χ_{FH} representing amorphous–amorphous interaction between the pair is generally assumed to be inversely proportional to the absolute temperature, i.e., $\chi_{FH} = A + B/T$, where A is related to athermal entropic correction and B represents enthalpic contribution. The non-equilibrium snapshots of the phase diagram during the course of polymerization reaction were calculated using the instantaneous volume fractions of the monomer and the polymer formed from it.

$$\alpha = \frac{\phi_2 - \phi_m}{\phi_2}, \quad \phi_p = \alpha\phi_2, \quad \phi_m = (1-\alpha)\phi_2 \tag{7}$$

where $\phi_m + \phi_p = \phi_2$ and $\phi_1 + \phi_2 = 1$ because of incompressibility assumption.

The free energy density of nematic ordering can be described according to Maier–Saupe mean-field theory [24].

$$g^{MS} = \frac{G^{MS}}{nkT} = \frac{\phi_1}{r_1}\left(\int f(\theta)\ln[4\pi f(\theta)]\mathrm{d}(\cos\theta) - \frac{1}{2}\nu\phi_1 s^2\right) \tag{8}$$

where s is the orientational order parameter, and $f(\theta)$ and ν represent the director distribution function and quadruple interaction parameter which can be expressed as

$$f(\theta) = \frac{1}{Z}\exp\left[-\frac{u(\theta)}{kT}\right] \tag{9}$$

$$\nu = 4.541\frac{T_{NI}}{T} \tag{10}$$

where Z is the partition function as defined below:

$$Z = \int \exp\left[-\frac{u(\theta)}{kT}\mathrm{d}(\cos\theta)\right] \tag{11}$$

The potential of a director orientation, $u(\theta)$, can be taken to be proportional to the second order Legendre polynomials, viz.,

$$\frac{u(\theta)}{kT} = -\frac{1}{2}m\left(3\cos^2\theta - 1\right) \tag{12}$$

in which m is dimensionless mean-field strength. By minimizing the free energy with respect to the orientational order parameter, the mean-field strength (m) can be related to the order parameter (s) and the anisotropic interaction parameter (ν), i.e., $m = \phi\nu s$. This relation leads to

$$g^{MS} = \frac{G^{MS}}{nkT} = \frac{\phi_1}{r_1}\left(-\ln Z + \frac{1}{2}\nu\phi_1 s^2\right) \tag{13}$$

Once the nematic–isotropic transition has been known, the coexistence curve may be established via self-consistent solution by equating the chemical potentials of each phase, viz. $(\partial f/\partial n)|_\alpha = (\partial f/\partial n)|_\beta$. The detailed calculation for the phase diagram can be found in our previous papers [2,25].

4. Results and discussion

4.1. Kinetic effects

In order to establish a relationship between emerged morphology of the films and the system variables such as temperature, irradiation intensity, monomer functionality and concentration, the role of the cure kinetics of photopolymerization on phase separation dynamics and concomitant morphological evolution needs to be investigated. Prior to exploring the kinetic parameters for the photopolymerization of multifunctional monomers and the effect of each competitive experimental parameter on LC domain morphology in relation to kinetics of phase separation, we investigate the kinetics of photopolymerization of neat acrylate monomers.

Fig. 2(a) illustrates IR spectra of PETA collected by real-time IR (RT-IR), subjected to irradiation at 40 °C for 1 min using the green laser (532 nm). The change in the peak area at 804 cm^{-1}, which corresponds to the stretching of the acrylate double bonds, is monitored for the conversion calculation. Fig. 2(b) shows the disappearance of the acrylate double bonds with photopolymerization of neat TMPTA and its mixture. Initial portion of the curve involves a rapid decrease in rate due to increase in the polymerization rate and then levels off when the conversion reaches its maximum value.

Based on the double-bond conversion by the RT-IR technique, the propagation and termination rate coefficients (k_p and k_t) of neat TMPTA were determined by irradiating the green laser (Fig. 3(a)). From 0 to 10% conversion, the

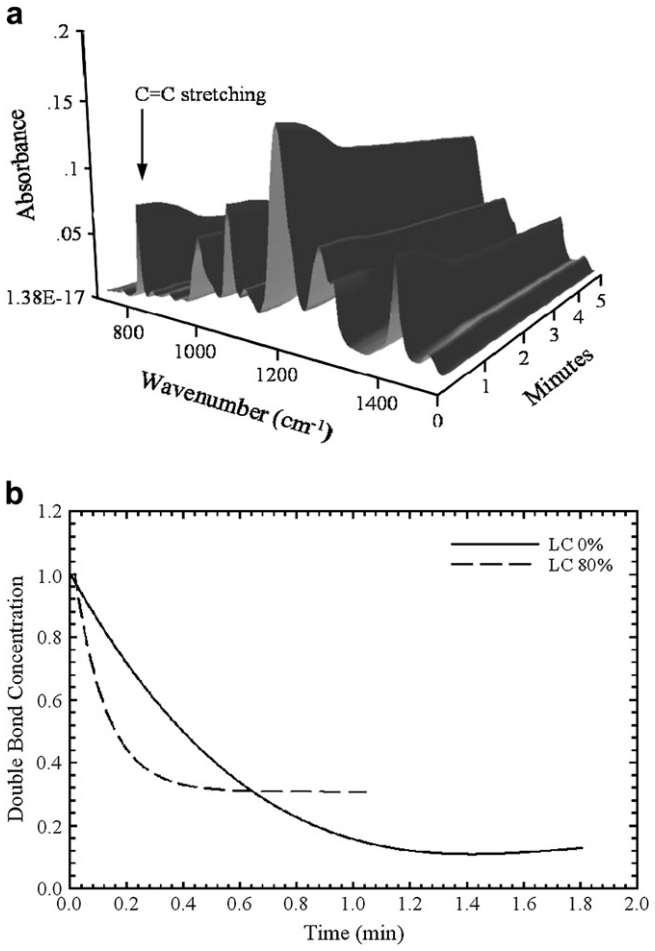

Fig. 2. (a) RT-IR spectra of PETA irradiated for 1 min at 40 °C with green laser at 532 nm and (b) influence of LC concentration on the photopolymerization of TMPTA with green laser irradiation (19 mW/cm^2, 532 nm) at 40 °C.

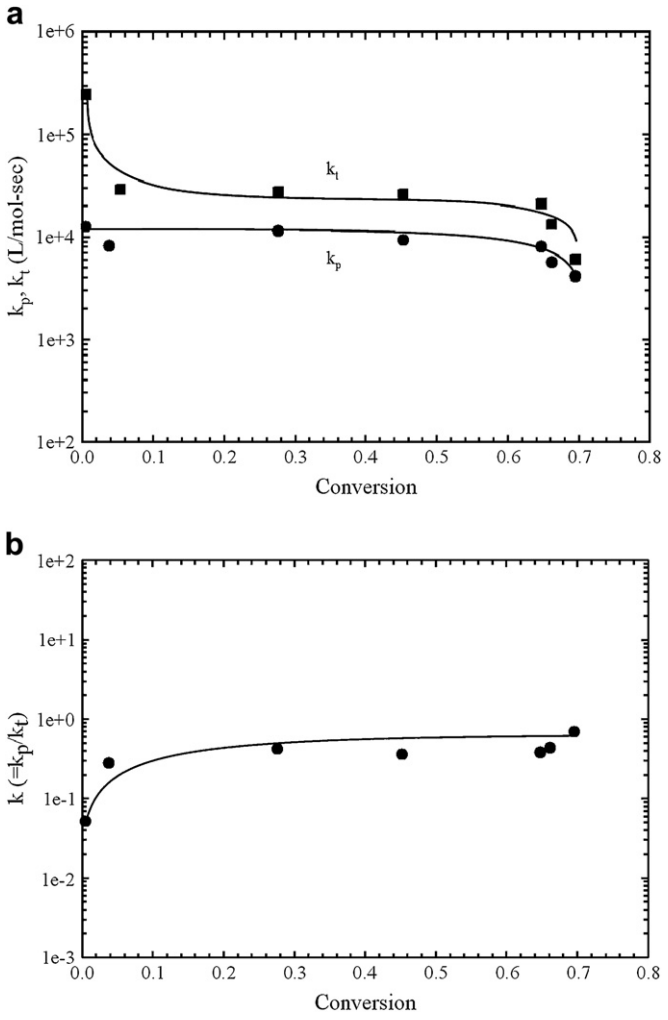

Fig. 3. Kinetic coefficients: (a) propagation rate and termination rate coefficients and (b) ratio $k = k_p/k_t$ for neat TMPTA as a function of double-bond concentration explored with RT-IR (intensity 19 mW/cm^2 at 40 °C at 532 nm).

termination rate coefficient decreases rapidly as the diffusion of macroradical chains becomes limited, while propagation remains unhindered. Subsequently, the trend of termination rate coefficient versus conversion becomes similar to that of the propagation rate coefficient, showing an invariant behavior with conversion. However, beyond 60%, both rate coefficients drop, which implies the prevalence of the cross-linking reaction. The shape of k_p and k_t as a function of conversion was thoroughly analyzed experimentally and theoretically by Anseth et al. [26–28]. As shown in Fig. 3(b), the ratio k_p/k_t initially increases with conversion and then it levels off. It may be inferred that the lumped rate coefficient k remains constant with conversion, except for the very early stage of the reaction. It is well known that the termination rate coefficient (k_t) is characterized by the diffusion-controlled process, but its diffusion mechanisms are different depending on the extent of the conversion. According to Anseth and coworkers [26–28], the initial rise at the low conversion region is attributable to the dominance of the segmental diffusion (i.e., reorientation of polymer segments bringing radical chain ends in a reaction zone). Reaction diffusion occurs when relatively immobile radicals propagate through a matrix of unreacted functional groups and monomers until encountering a second radical for termination, and in this region the termination is proportional to the propagation. As a consequence, a plateau region can be discerned in the lumped reaction coefficient versus conversion plot. Hence, the plateau region at the higher conversions may be interpreted as the signature of the reaction diffusion dominating in the termination step.

Fig. 4 presents the influence of the acrylate functionality (f) on the kinetics of photopolymerization as obtained by RT-IR. When the functionality rose from 3 to 4, the maximum polymerization rate increased as expected. However, we were first puzzled by the fact that the maximum polymerization rate for DPEPHA ($f = 5$) was located inbetween those of TMPTA ($f = 3$) and PETA ($f = 4$). It turns out that the pure DPEPHA is a very viscous liquid and it was supplied by adding a small amount of TMPTA and PETA in order to improve the flowability, and thus the observed behavior of the polymerization rate with respect to the conversion is no longer at odd to each other.

The termination (k_t) and propagation (k_p) behaviors for a series of TMPTA, PETA and DPEPHA were further determined

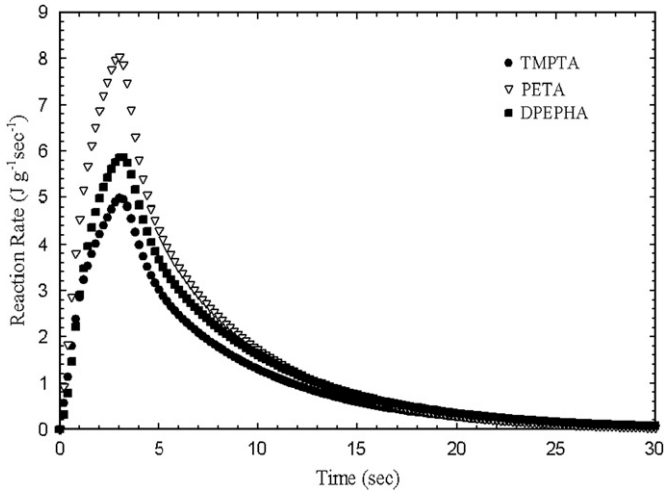

Fig. 4. P-DSC trace of reaction rate versus time for neat TMPTA, PETA and DPEPHA monomers during the photopolymerization under the UV irradiation with 44.5 mW/cm^2 and 365 nm at 50 °C.

by means of the P-DSC technique. Since the conversion was examined by UV sources with different intensities (44.5 mW/cm^2 at 365 nm), the trends are somewhat different from those obtained from RT-IR (19 mW/cm^2 at 532 nm). The termination rate coefficient (k_t) shows a sharp decrease from the very beginning of polymerization for all functionalities (Fig. 5(b)). In general, as the functionality of the monomer is increased, the average cross-linked density of the system is increased. This increased cross-linking led to an earlier dominance of the reaction diffusion, causing a lower value for the termination rate coefficient for higher functionality monomers. The propagation rate coefficient (k_p), on the other hand, shows a sudden increase at the initial stage of the irradiation. This may be attributed to the onset of autoacceleration. After around 2% conversions, the propagation step is dominated by the diffusion-controlled (autodeceleration) process, and then k_p decreased asymptotically (Fig. 5(a)). It seems that a large concentration of radicals is created within a very short time span upon exposure to UV radiation. This greatly enhances the chain propagation at the beginning and leads to a large propagation rate constant. After the gel point (maximum k_p), propagation is hindered drastically causing a sharp decline in the rate constants. For all functionalities, the gel point may occur near 2% of double-bond conversions although it was hard to precisely identify the composition of gel point owing to the slow response of P-DSC. As depicted in Fig. 5(c), the ratio $k = k_p/k_t$ increases at low conversions and then reaches a plateau regardless of monomer functionality. This observation is consistent with the RT-IR results of Fig. 3(b) and also with those of Anseth et al. [26–28] as well as by Andrzejewska [15]. According to Andrzejewska, the observed trend of $k = k_p/k_t$ with conversion may be explicable in terms of the mixed monomolecular and bimolecular terminations. It should be pointed out that the plot of k versus conversion based on the bimolecular termination assumption, i.e. ($k = k_p/k_t^{1/2}$), turns out to be inadequate to account for the present multifunctional acrylate monomers.

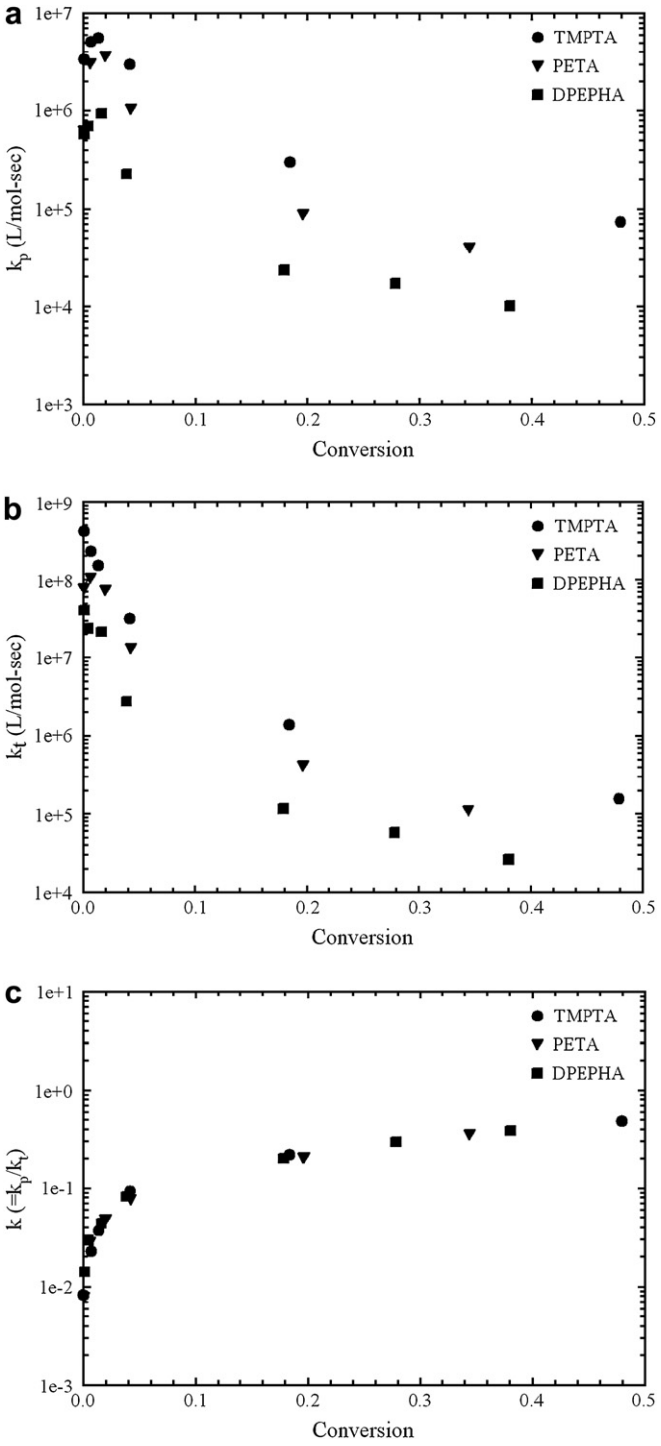

Fig. 5. Dependence of (a) propagation rate and (b) termination rate coefficients, (c) ratio $k = k_p/k_t$ on the double-bond conversion for neat TMPTA, PETA, and DPEPHA monomers irradiated with an UV light at 44.5 mW/cm^2 and 50 °C.

4.2. Effect of light intensity

The relative contributions of monomolecular and bimolecular terminations can be estimated based on the light intensity exponent. The classical kinetic model given by Tryson and Shultz [29] has been widely used for the kinetic analysis of free radical

photopolymerization. With the incorporation of additional kinetic features, the model has made considerable advances over the last three decades and it appears adequate for describing general linear photopolymerization under steady state. Recent experimental observations indicate that the classical kinetic model fails to predict reaction kinetics accurately over a range of multifunctional monomers undergoing monomolecular termination or radical trapping and cyclization reactions [30–34]. According to the classical kinetic model, the polymerization rate is treated to be proportional to the square root of I_a at equal monomer conversions as shown in Eq. (14),

$$-\frac{d[M]}{dt} = k[M][\Phi I_a]^m \tag{14}$$

where m is the reaction exponent and k is lumped rate constant given as $k = k_p/k_t^n$. In the classical kinetic model [29], n is taken as 0.5 because of the inherent assumption of bimolecular termination reaction between macroradicals. In a previous paper, we reported that $I_a^{0.5}$ was valid only in the initial stage of the reaction, but at the steady state, where termination by trapping is competing with termination by combination, k changes according to I_a, i.e., $n = 1$ [35].

Fig. 6(a) illustrates the dependence of the maximum polymerization rate of TMPTA on the absorbed light intensity at various conversions. Three different intensities, 44.5, 71, and 150 mW/cm^2 (at 365 nm wavelength), were used. Experimental data plotted in logarithmic scale exhibit the exponent value in the range $m = 0.82–0.94$ over the whole conversion region (Fig. 6(b)). The exponent values between 0.5 and 1 for the multifunctional acrylate polymerizations have been proposed by other groups [21,36]. If the monomolecular termination were occurring exclusively, the value of unity would be expected. Decker and Moussa [21] confirmed the linear first-order relationship dependence between R_p and the intensity of a multifunctional polyurethane–diacrylate monomer and photoinitiator (i.e., IC-651). However, in practice most of the multifunctional monomer systems do not show linear or square root dependence due to the simultaneous occurrence of monomolecular and bimolecular terminations as well as cyclization reactions. From the observed rate coefficients (k_p and k_t) and its ratio $k = k_p/k_t$ as well as the exponent value (m) being in the range 0.82–0.94, it may be inferred that the combined monomolecular and bimolecular termination mechanisms may be more reasonable to account for the termination process of the present multifunctional monomers. With this acquired knowledge of the photopolymerization behavior of the multifunctional acrylate systems, we shall explore the morphological development in relation to the snapshot phase diagram of the polymerizing LC/acrylate monomer system.

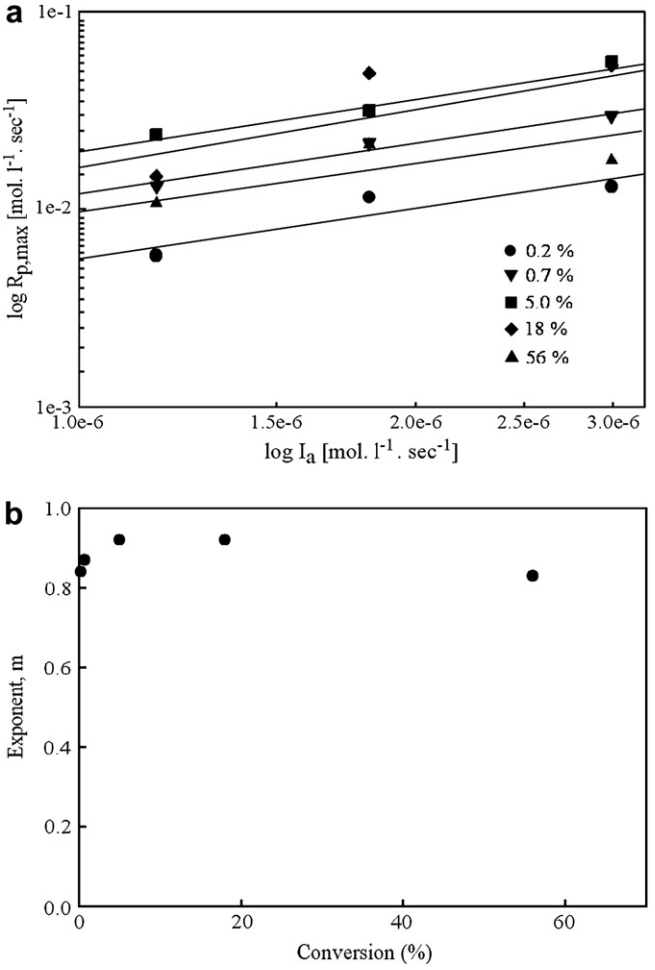

Fig. 6. (a) Maximum rate of polymerization, $R_{p,max}$, as a function of absorbed light intensity, I_a, for neat TMPTA at 0.2, 0.7, 5, 18 and 56% conversion and (b) plots of exponent by which polymerization rate is proportional to the absorbed light intensity. Incident light intensities: 44.5, 71, 150 mW/cm^2 at 365 nm wavelength.

4.3. Phase diagram before polymerization

The phase diagram of monomer/LC mixture gives thermodynamic stability limits of the starting mixture as a function of temperature and composition. Depending on the photopolymerization conditions (i.e., concentration and reaction temperature), the emerged morphology can be profoundly influenced [8,37]. Therefore, it is essential to establish the phase diagram of the reactive monomer/LC system as a guide for kinetic pathways.

The theoretical coexistence curve was calculated self-consistently in accordance with the combined Flory–Huggins and Maier–Saupe theory. The material parameters utilized in the calculation were $r_1 = 1$, $r_2 = 1$, $A = 0$, and $T_{NI} = 61$ °C. Fig. 7 demonstrates the effect of RBAX initiator on the nematic–isotropic transition temperature prior to photopolymerization. The solid lines represent the theoretical phase diagrams of the TMPTA/E7 system. Note that the liquid–liquid phase separation (e.g., upper critical solution temperature, UCST) is not clearly discernible in the phase diagram, because it is buried underneath the mesophase–liquid phase transition curves (i.e., liquidus lines). It is seen that the addition of a small amount of photoinitiator suppresses the liquidus line as compared to those of the LC/monomer blend containing no RBAX initiator. The depression becomes more pronounced especially at low LC concentrations (<50% LC). This

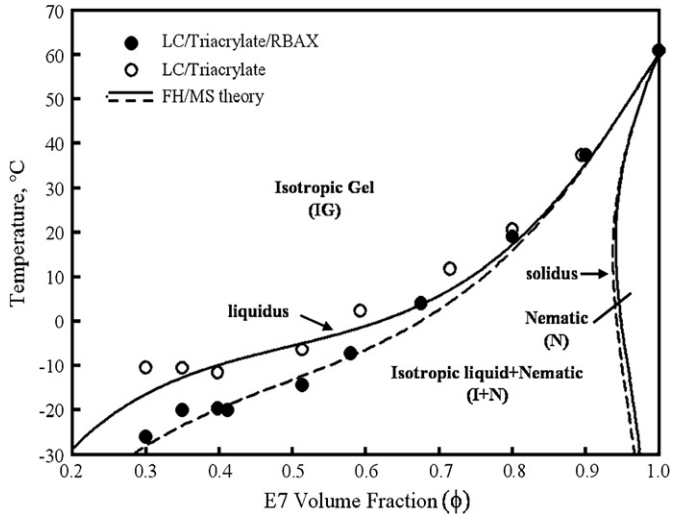

Fig. 7. Phase diagram for TMPTA/E7 system with and without containing Rose Bengal (RBAX) curatives. The points indicate the phase transition temperatures as obtained by differential scanning calorimetry (DSC). The solid lines are the snapshots obtained via the self-consistent solutions of the coexistence curves. IG represents isotropic gel and I + N stands for the coexistence region of isotropic liquid + nematic phase.

declining trend is expected because a larger amount of initiators were needed for the higher monomer concentrations (or low LC compositions). Note that the equimolar amount of initiator was used on the basis of the monomer weight fraction of the LC/monomer mixture. This T_{NI} depression may be attributed to the plasticization effect. A similar initiator effect was found by Kim et al. [38], which was interpreted due to the increase in polymer solubility of LC with increasing photoinitiator concentration.

4.4. Effect of liquid crystal concentrations on photopolymerization kinetics

The propagation and termination coefficients of TMPTA/E7 blends were determined using the green laser. As shown in Fig. 8, the rate constants decline rapidly with increasing LC concentration, but there is no systematic trend in the variation of the reaction rate coefficients versus conversion (Fig. 8(a) and (b)). Although increasing LC content enhances the mobility (or mutual diffusion), while providing more accessible space for the polymerization of acrylate to occur, the reaction coefficient value drops drastically and also the extent of conversion reduces significantly (Fig. 2(b)). Once phase separation occurs, some unreacted monomers could be trapped within the LC-rich region and thus the probability of collision between the growing polymers and the residual monomers is diminished. Moreover, the acrylate monomer concentrations in the LC-rich phase would be low leading to incomplete conversion. As can be noticed in Fig. 8(c), the lumped rate coefficient, $k = k_p/k_t$, fluctuates severely, showing no clear trend, except its value is in the comparable range of those obtained for the neat multifunctional acrylates. The inconsistent trends of the k_p and k_t values versus conversion

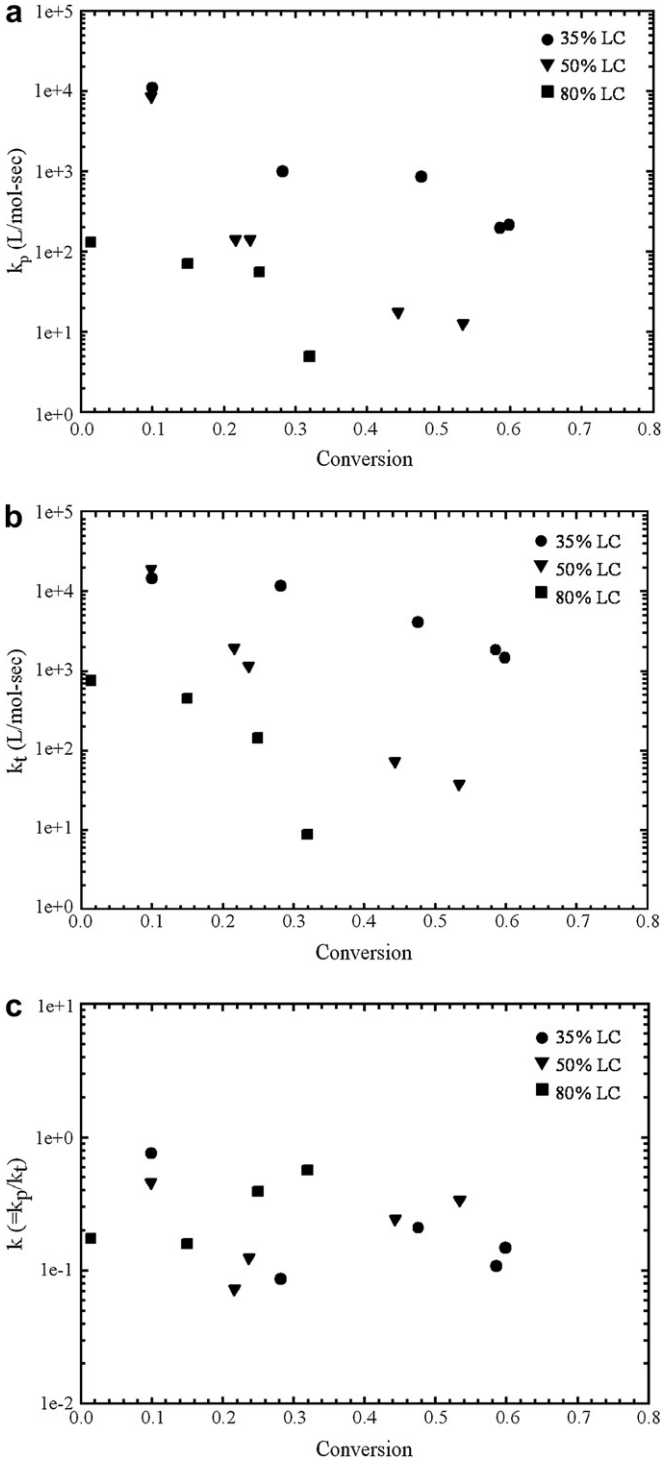

Fig. 8. Kinetic coefficients: (a) propagation rate and (b) termination rate coefficients, (c) ratio $k = k_p/k_t$ for TMPTA/E7 mixtures as a function of double-bond concentration explored with RT-IR (intensity: 19 mW/cm^2, at 40 °C at 532 nm). TMPTA with (●) 35%, (▼) 50%, and (■) 80% LC concentration.

and the large fluctuations of $k = k_p/k_t$ with the addition of LC may be attributed to sample turbidity caused by possible phase separation and/or LC director fluctuations.

In this study, two complementary techniques, viz., P-DSC and RT-IR, were employed to evaluate the kinetic coefficients.

The majority of PDLC films is fabricated by irradiating either by a green laser or by an UV light or both. P-DSC technique measures the total heat evolved during photopolymerization. Although the released heat may be taken to be directly proportional to the number of monomer units reacted (i.e., the number of C=C bonds), there is another contribution of heat release due to initiation reactions (light absorption). Therefore, the reaction enthalpy liberated to the P-DSC thermograms involves the complex contributions of heat release by various photopolymerization steps. In the case of RT-IR techniques, it affords the direct measurement of the reaction through the depletion of C=C bonds. However, the turbidity due to phase segregation (i.e., concentration fluctuation) and nematic ordering (i.e., director fluctuation) makes the IR absorption to fall below the Beer–Lambert limit. Moreover, RT-IR at 532 nm irradiation gave a slightly lower final conversion than that of P-DSC due to the aforementioned problem of the blend turbidity.

4.5. Evolution of phase diagram during photopolymerization

The nematic–isotropic transition temperatures of the polymerized blends were determined by DSC as a function of irradiation time and then compared to theoretical calculation. In Fig. 9, two regions can be identified in the descending order of temperature, i.e., isotropic gel (IG) or swollen network, and isotropic liquid + nematic (I + N) solvent. The snapshots (non-equilibrium) of the NI transition temperatures (T_{NI}s) with reaction times reveal the enhanced NI transition at all blend concentrations with increasing exposure time. It is noticed that the T_{NI} versus volume fraction curve (i.e., liquidus line) appears to bulge asymmetrically to the right hand side, which may be a consequence of the UCST envelop

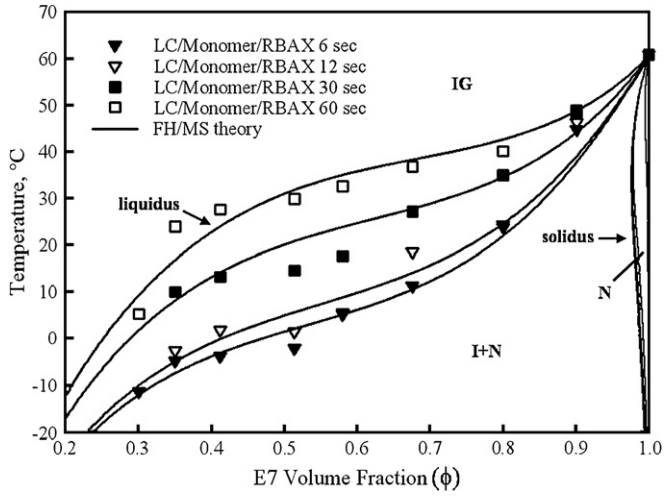

Fig. 9. Evolution of the coexistence curves as a function of UV exposure time after irradiation at the light intensity of 50 mW/cm^2. The points indicate the phase transition temperatures as obtained by differential scanning calorimetry (DSC). The solid lines are the snapshots obtained via the self-consistent solutions of the coexistence curves.

moving upward. These changes in the phase diagram by photopolymerization imply that the monomer in the LC-rich phase is gradually separated out and gets polymerized with increasing UV exposure time. As molecular weight increases upon photopolymerization, the emerging polymers become less soluble in the LC-rich phase. When the reduction in miscibility supercedes the plasticization effect, the UCST gap expands, thereby giving rise to an increase in the liquidus line (or the depressed T_{NI} line). Note that the observed T_{NI} line is the consequence of the competition between the liquid–liquid phase separation and the solid–liquid phase transition of the nematic constituent. This effect is less pronounced for high LC mixtures (≥80% LC), because the reactive monomer amount is very little to affect the coexistence points.

4.6. Morphological development

Based on the experimental and theoretical phase diagrams, morphological evolution was investigated during photopolymerization at different temperatures. Fig. 10 shows the optical micrographs depicting the morphological evolution of TMPTA/E7 mixtures as a function of LC concentration upon exposing to UV irradiation at 50 mW/cm^2 in the isotropic phase (50 °C). During the photocuring, the mixture undergoes phase separation driven by the increase in the molecular weight of the growing polymer. Subsequently, the polymeric network forms (polymer-rich region) and the liquid crystals and the unreacted monomers (LC-rich region) are segregated within the network. The diffusion of the LC molecules through the highly viscous network medium is rather slow, thereby hampering the domain growth. Upon cooling into the two-phase gap (23 °C), liquid crystal molecules reorganize and form nematic structures, showing the segregated tiny nematic LC droplets within the polymer matrix. As the polymerization progresses, nematic ordering occurs simultaneously with phase separation and nematic textures develop within the phase separated domains. With continued photopolymerization reaction, vitrification sets in and thus the growth of the LC domain is practically ceased.

When photopolymerization was performed in the biphasic region (at 30 °C), which is below phase transition temperature of the LC/polymer mixtures, the mixture gave rise to inhomogeneous films (Fig. 11), revealing birefringent texture characteristics of the nematic liquid crystals. The average length scale of these LC domains is non-uniform and larger than those obtained during photopolymerization at 50 °C (Fig. 10). At 50–80% of LC compositions, the dispersed LC droplets can be seen clearly. Under the unpolarized geometry, numerous line and/or point disclinations can be discerned within these LC domains. It appears that phase separation dominates over the curing kinetics, leading to the formation of large and irregularly shaped LC domains having a wide distribution of domain sizes. At 90% of LC concentration, the polymer-rich phase clearly exhibits schlieren textures, indicative of the nematic LC disclination. The aforementioned POM observations suggest that the selection of initial

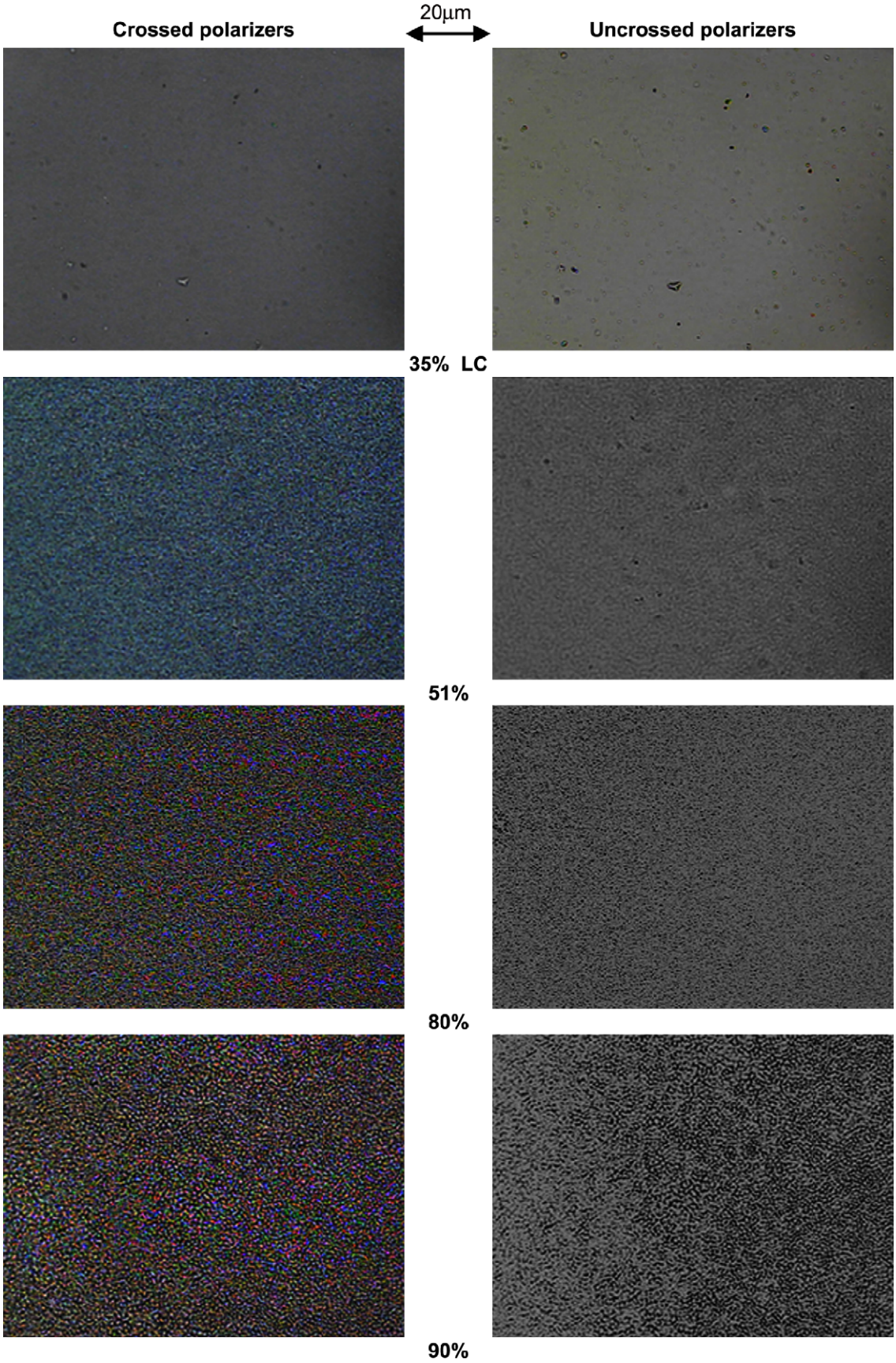

Fig. 10. Polarized optical microscopic images of several TMPTA/E7 mixtures following photopolymerization in the single-phase region (50 °C) and then cooling to 23 °C using crossed (left) and uncrossed (right) polarizers.

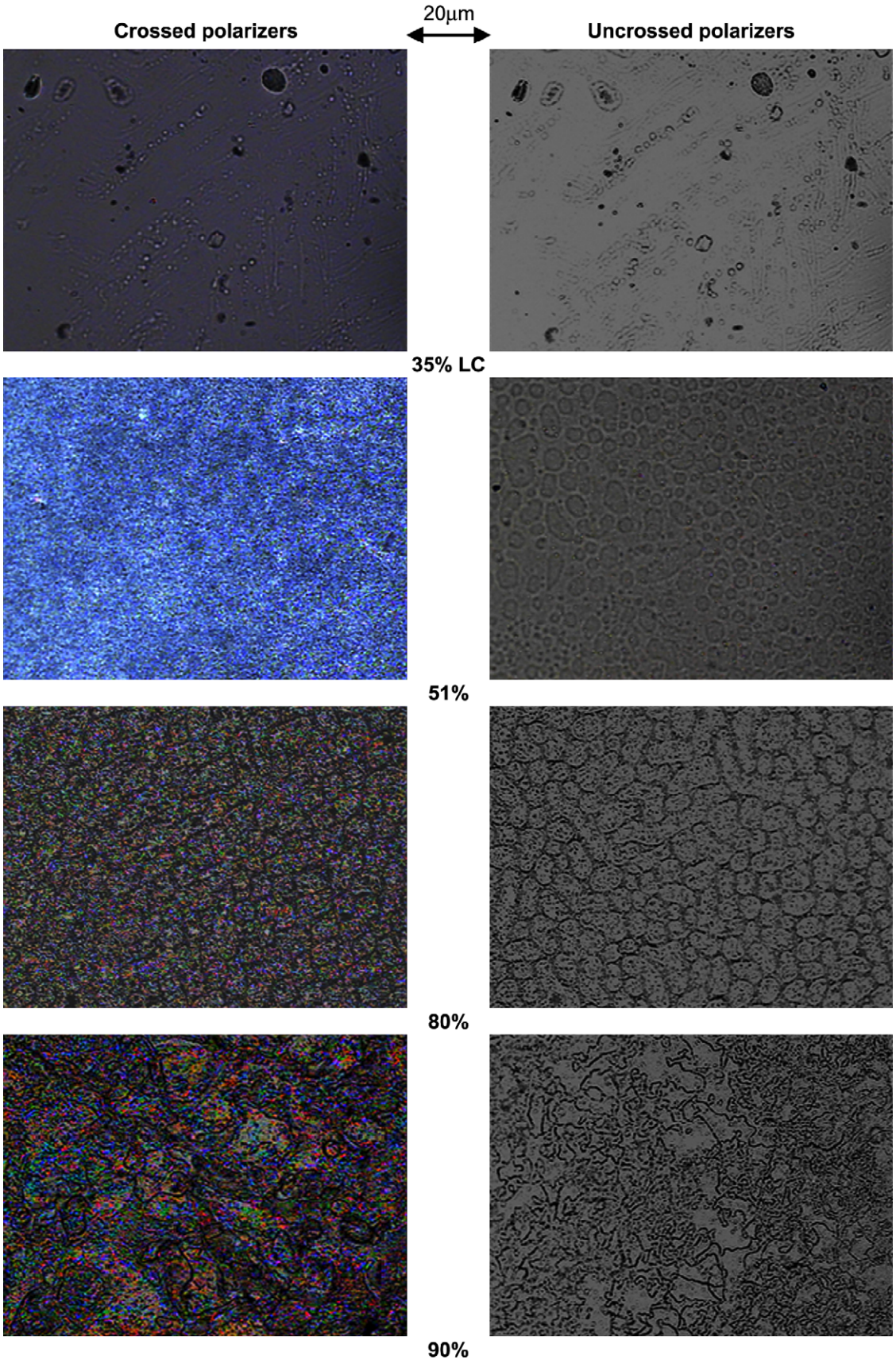

Fig. 11. Polarized optical microscopic images of several TMPTA/E7 mixtures following photopolymerization at 30 °C and then cooling to 23 °C using crossed (left) and uncrossed (right) polarizers, showing the development of nematic domains.

composition and reaction temperatures in reference to the LC/monomer phase diagram are critical for controlling the emerged LC textures as well as the domain size, which may adversely affect the electro-optical performance of the PDLC film.

5. Conclusions

Although the trends of propagation (k_p) and termination (k_t) with conversion appear slightly different between RT-IR and P-DSC techniques utilized, the lumped rate constant ($k = k_p/k_t$) shows a consistent trend in neat multifunctional monomers. Moreover, the observed exponent value ($m = 0.82-0.94$) of I_a implies that the combined monomolecular and bimolecular termination mechanisms may be most reasonable for describing the termination steps of multifunctional monomers. However, upon addition of LCs, the decaying trends of the k_p and k_t values with conversion show some deviations from those of the pure monomer case, leading to the large fluctuations of the lumped rate constant, which may be attributed to sample turbidity caused by possible phase separation of the blends and the concomitant LC director fluctuations.

The phase diagram thus established experimentally and theoretically exhibits various coexistence phases including isotropic gel (IG), isotropic liquid + nematic (I + N) solvent, and pure nematic (N). The non-equilibrium evolution of the NI transition temperatures (T_{NI}s) with the progression of the reaction reveals the enhanced NI transition at all blend concentrations with increasing exposure time. The morphological development in the single phase showed the development of uniform LC domains, whereas the blends photopolymerized in the two-phase region produced larger and irregular LC domain shapes, implying that photopolymerization conditions such as the choice of reaction temperatures and concentrations profoundly affect the resulting PDLC morphology.

Acknowledgments

The authors express their gratitude to the supports of the National Science Foundation through Grant # DMR 0514942, and of the Collaborative Center for Polymer Photonics (CCPP), sponsored by Air Force Office of Scientific Research, Wright–Patterson Air Force, and the University of Akron.

References

[1] White TJ, Liechty WB, Natarajan LV, Tondiglia VP, Bunning TJ, Guymon CA. Polymer 2006;47:2289–98.
[2] Meng S, Duran H, Kyu T. J Phys Chem 2007;111:5116–23.
[3] Doane JW. In: Bahdur B, editor. Liquid crystals: applications and uses. Singapore: World Scientific; 1991.
[4] Doane JW, Golemme A, West JL, Whitehead JB, Wu B-G. Mol Cryst Liq Cryst 1988;165:511–32.
[5] Lovinger AJ, Amundson KR, Davis DD. Chem Mater 1994;6:1726–36.
[6] Rajaram CV, Hudson SD, Chien LC. Chem Mater 1995;7:2300–8.
[7] Guymon CA, Hoggan EN, Walba DM, Clark NA, Bowman CN. Liq Cryst 1995;19:719.
[8] Nwabunma D, Chiu H-W, Kyu T. Macromolecules 2000;33:1416–24.
[9] Hoyle CE, Chawla CP, Kang D, Griffin AC. Macromolecules 1993;26:758–63.
[10] Kim BK, Cho YH, Lee JS. Polymer 2000;41:1325–35.
[11] Rajaram CV, Hudson SD, Chien LC. Polymer 1998;39:5315–9.
[12] Valdes-Aguilera O, Pathak JS, Watson D, Neckers DC. Macromolecules 1992;25:541–7.
[13] Bunning TJ, Natarajan LV, Tondiglia VP, Sutherland RL. Annu Rev Mater Sci 2000;30:83–115.
[14] Du H, Fuh RA, Li J, Corkan A, Lindsey JS. Photochem Photobiol 1998;68:141–2.
[15] Andrzejewska E. Macromol Symp 2001;171:243–52.
[16] Khudyakov IV, Legg JC, Purvis MB, Overton BJ. Ind Eng Chem Res 1999;38:3353–9.
[17] Pappas SP. Radiation curing: science and technology. New York: Plenum Press; 1992. p. 57–151.
[18] Decker C. Acta Polym 1994;45:333–47.
[19] Decker C, Moussa K. Macromolecules 1989;22:4455–61.
[20] Decker C. J Coat Technol 1990;62:55–61.
[21] Decker C, Moussa K. Macromol Chem 1988;189:2381–94.
[22] Flory PJ. J Chem Phys 1942;10:51–61.
[23] Huggins ML. J Chem Phys 1941;9:440.
[24] Maier W, Saupe A. Z Naturforsch 1958;A13:564–6; 1959;A14:882–9; 1960;A15:287–92.
[25] Nwabunma D, Kyu T. Macromolecules 1999;32:664–74.
[26] Anseth KS, Wang CM, Bowman CN. Macromolecules 1994;27:650–5.
[27] Anseth KS, Wang CM, Bowman CN. Polymer 1994;35:3243–50.
[28] Anseth KS, Bowman CN. Polym React Eng 1993;1:499–520.
[29] Tryson GR, Shultz AR. J Polym Sci Polym Phys Ed 1979;17:2059–75.
[30] Batch GL, Macosko CW. J Appl Polym Sci 1992;44:1711–29.
[31] Decker C, Moussa K. J Polym Sci Part A Polym Chem 1987;25:739–42.
[32] Wen M, McCormick AV. Macromolecules 2000;33:9247–54.
[33] Kloosterboer JG, Van de Hei GMM, Gossink RG, Dortant GC. Polym Commun 1984;25:322–5.
[34] Elliot EJ, Nie J, Bowman CN. Polymer 2003;44:327–32.
[35] Meng S, Duran H, Hu J, Kyu T, Natarajan LV, Tondiglia VP, et al. Macromolecules 2007;40:3190–7.
[36] Karzmarek H, Decker C. J Appl Polym Sci 1994;54:2147–56.
[37] Nwabunma D, Kim K-J, Lin Y, Chien L-C, Kyu T. Macromolecules 1998;31:6806–12.
[38] Kim BK, Kim SH, Song JC. Polymer 1998;39:5949–59.